Wind and Structures, *Vol. 30, No. 2 (2020) 181-198*
DOI: https://doi.org/10.12989/was.2020.30.2.181

Investigation on spanwise coherence of buffeting forces acting on bridges with bluff body decks

Qi Zhou*[1], Ledong Zhu[2a], Chuangliang Zhao[2b] and Pengjie Ren[2c]

[1]*Guangdong Engineering Center for Structure Safety and Health Monitoring, Shantou University, No.243 Daxue Road, Shantou, Guangdong Province, China*
[2]*State Key Laboratory for Disaster Reduction in Civil Engineering, Tongji University, No.1239 Siping Road, Shanghai, China*

(Received February 4, 2019, Revised October 16, 2019, Accepted November 4, 2019)

Abstract. In the traditional buffeting response analysis method, the spanwise incomplete correlation of buffeting forces is always assumed to be same as that of the incident wind turbulence and the action of the signature turbulence is ignored. In this paper, three typical bridge decks usually adopted in the real bridge engineering, a single flat box deck, a central slotted box deck and a two-separated paralleled box deck, were employed as the investigated objects. The wind induced pressure on these bridge decks were measured via a series of wind tunnel pressure tests of the sectional models. The influences of the wind speed in the tests, the angle of attack, the turbulence intensity and the characteristic distance were taken into account and discussed. The spanwise root coherence of buffeting forces was also compared with that of the incidence turbulence. The signature turbulence effect on the spanwise root coherence function was decomposed and explained by a new empirical method with a double-variable model. Finally, the formula of a sum of rational fractions that accounted for the signature turbulence effect was proposed in order to fit the results of the spanwise root coherence function. The results show that, the spanwise root coherence of the drag force agrees with that of incidence turbulence in some range of the reduced frequency but disagree in the mostly reduced frequency. The spanwise root coherence of the lift force and the torsional moment is much larger than that of the incidence turbulence. The influences of the wind speed and the angle of attack are slight, and they can be ignored in the wind tunnel test. The spanwise coherence function often involves several narrow peaks due to the signature turbulence effect in the high reduced frequency zone. The spanwise coherence function is related to the spanwise separation distance and the spanwise integral length scales, and the signature turbulence effect is related to the deck-width-related reduced frequency.

Keywords: buffeting force; root coherence function; empirical model; signature turbulence; incident wind turbulence

1. Introduction

Many innovative long-span cable-stayed and suspension bridges have been built or planned in recent years. These long span bridges are usually related to bridges with a main span length of approximately 1000 m or longer. The maximum span cable-stayed bridge that has been reached, up to now, is Russky Island Bridge with a main span of 1104 m located in Vladivostok in Russia, while the maximum span suspension bridge that was ever built is the Akashi Kaikyo Bridge in Japan, with a mains span of 1990m. For these long-span bridges, the flexibility is high, and the first natural frequency is about 0.1 Hz or lower. In this regard, these long-span bridges are sensitive to the wind action and the wind action becomes the major problem in their overall design. Buffeting is an important stochastic vibration induced by the wind and it is indispensable for the wind resistance design of long-span bridges (Chen *et al.* 2009). Scientists and engineers are thus playing more and more attention to the accuracy prediction of the buffeting response.

The traditional buffeting analysis of long-span bridges has been performed for almost 50 years. Davenport first presented the framework for buffeting analysis of long-span bridges by introducing the theory of statistics and stochastic vibration (Davenport 1962). Scanlan then introduced flutter derivatives into the buffeting analysis to account for the self-excited forces (Scanlan 1978). After the endeavors of the predecessors for decades, the effects of multi-modes and inter-mode coupling can now be analyzed with fully-coupled 3D buffeting analysis methods (Jain *et al.* 1996, Xu *et al.* 2000, Chen and Kareem 2002, Tubino and Solari 2007). In the recent decades, some new models of aerodynamic admittances, used to consider the unsteady effect of buffeting forces, were proposed and some new understandings about the aerodynamic admittances were achieved, i.e., the concept of 3D aerodynamic admittances (Costa 2007, Han *et al.* 2010, Ma *et al.* 2019, Li *et al.* 2019). The non-stationary buffeting responses of long-span bridges can be predicted or evaluated based on the force parameters from stationary wind (Hu and Xu, 2013; Chen, 2019). In order to analyze the fatigue of long-span bridges induced by buffeting response, the characteristics of distributed aerodynamic forces on bridge decks were

*Corresponding author, Associate Professor
E-mail: zhouqi@stu.edu.cn
[a]Professor
E-mail: ledong@tongji.edu.cn
[b]Master
E-mail: zhaochuanliangld@163.com
[c]Master
E-mail: pengjieyum@gmail.com

ISSN: 1226-6116 (Print), 1598-6225 (Online)

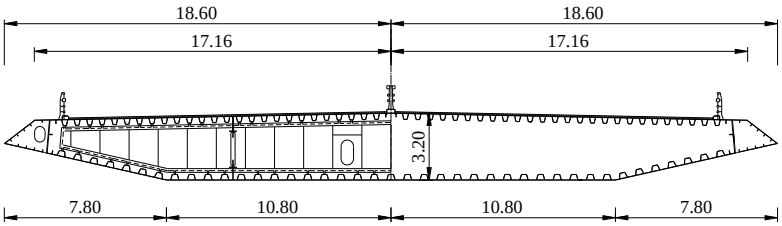

Fig. 1 Typical cross section of the third Nanjing Bridge in the main span (Unit: m)

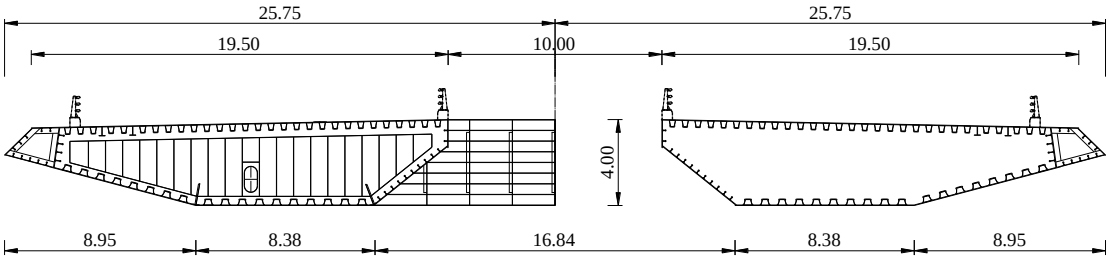

Fig. 2 Typical cross section of Shanghai Bridge in the main span (Unit: m)

investigated via a series of pressure measurement wind tunnel tests (Argentini *et al.* 2012, Zhu and Xu 2014). Thus, the stress-level buffeting analysis framework was proposed according to the distributed pressure around the bridge deck (Zhu and Xu 2016). In addition, buffeting response analysis of the long-span bridges under the construction stage was conducted and validated by the wind tunnel tests (Choi and Kim 2008, Won *et al.* 2008, Li *et al.* 2014).

However, in the traditional buffeting analysis approach, only the action of the incident wind turbulence is taken into account, and the behavior of the spanwise incomplete correlation of the buffeting forces is always assumed to be the same as that of the incident wind turbulence. In fact, many recent fruits and test results obtained by various researchers show that the spanwise correlation of the buffeting forces are much better than that of the incident wind turbulence (Jakobsen 1996, Larose 1997, Xu 2006). Some empirical formulas have been fitted and proposed via the wind tunnel tests and field measurements (Irwin 1977 Davenport *et al.* 1992, Hjorth-Hansen *et al.* 1992, Sankaran and Jancauskas 1993, Miyata *et al.* 2002). Moreover, in order to develop the framework of the stress-level buffeting analysis, the spanwise root coherences of the wind-induced pressures on the surface of bridge decks were reconstructed based on the method of POD (Tan *et al.* 2018). Nevertheless, the research regarding spanwise incomplete correlation of buffeting forces is still unclear and incomplete. This is especially true for the influence of signature turbulence on the spanwise correlation behaviors of buffeting forces on bluff body bridge girders, which has rarely been investigated and reported up to now.

In connection to this, the single flat box deck employed in the third Nanjing Bridge over the Yangtze River, the central slotted box deck adopted in the Shanghai Bridge over the Yangtze River, and the two-separated paralleled box deck used in the Tanggu Bridge over the Hai River were taken as examples to investigate the characteristics of the spanwise correlation of the buffeting forces in this study. A series of wind tunnel pressure tests were conducted via the sectional model in order to measure the wind-induced pressure on the bridge girders. In the wind tunnel tests, some possible influence factors were taken into account, such as the wind speed, the angle of wind attack, the wind turbulence intensity and the distance between cross sections of bridge girder. Afterward, by comparing the measurement results, the spanwise coherence characteristics of the buffeting forces were carefully analyzed and discussed. Finally, the signature turbulence effect was explained and discussed within a new analysis empirical model, and a double-variable model for the spanwise coherence of buffeting force was proposed.

2. Information of selected bluff body decks

2.1 The third Nanjing Bridge over the Yangtze River

The third Nanjing Bridge over the Yangtze River, located in Nanjing, Jiangsu province, China, is a two cable-plane cable-stayed bridge with a single flat box deck carrying dual three-lane highway traffic. The bridge is with a main span of 688 m and the typical cross section of the bridge deck in the main span is shown in Fig. 1. In this article, the cross section of the third Nanjing Bridge in main span, taken as the first investigated sample, is a typical single flat box deck which with 37.2 m in width and 3.2 m in height.

2.2 Shanghai Bridge over the Yangtze River

The Shanghai Bridge over the Yangtze River, located in Shanghai, China, is also a two cable-plane cable-stayed bridge carrying dual three-lane highway traffic. The bridge has a main span of 730 m, and its bridge deck in the main span is a central slotted box, which is shown in Fig. 2. The cross section of Shanghai Bridge in main span, taken as the second investigated sample, is with 51.5 m in width and 4.0 m in height.

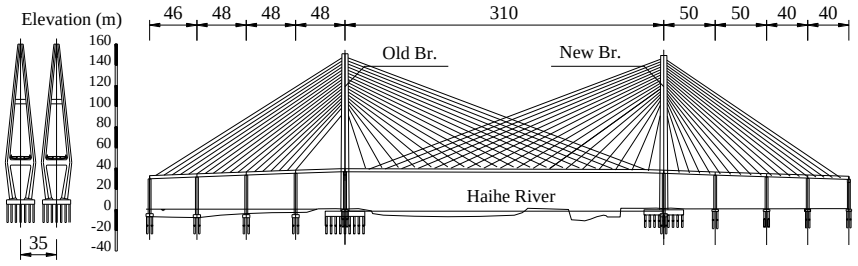

Fig. 3 Layout of the old and new Tanggu Bridges (Unit: m)

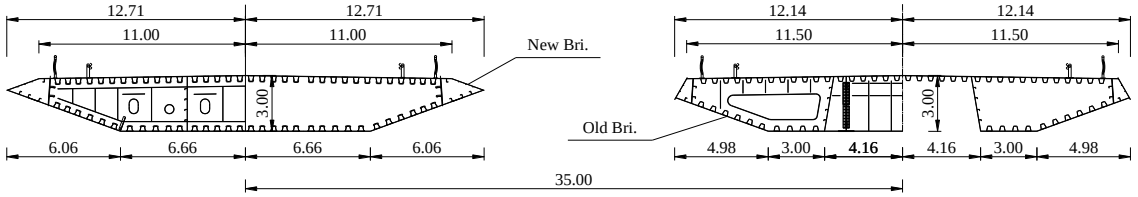

Fig. 4 Typical cross sections of the Tanggu Bridge in the main spans (Unit: m))

girders.

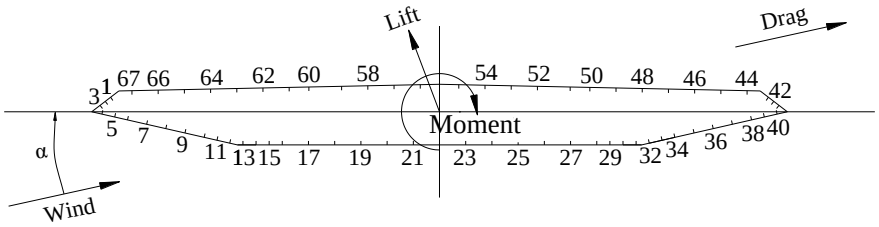

(a) Position and number of pressure-taps

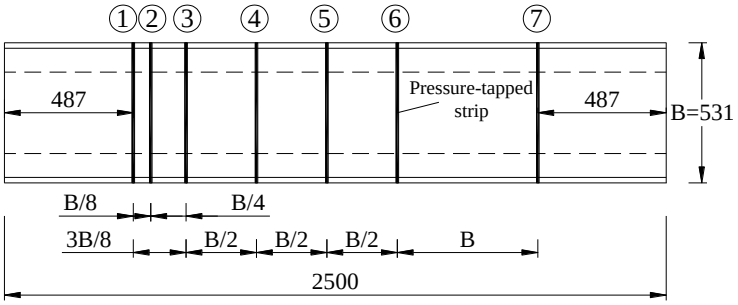

(b) Distribution of pressure-tapped strips

Fig. 5 Pressure strips and taps on the single flat box girder (Unit: mm)

2.3 Tanggu Bridge over the Hai River

The Tanggu Bridge over the Hai River, located in Tianjin, China, is composed of an existing bridge and a new constructed bridge. Both are two cable-plane cable-stayed bridges with single main towers and with main spans of 310 m. The layout of the old and new Tanggu Bridges is depicted in Fig. 3. The two bridges are similar in layout, including a semblable tower, the relatively same elevation of the bridge deck in the main span, the closely breadth of cross sections, etc. The typical cross section of the old bridge is a full-closed box and that of the new bridge is a semi-closed box. The distance between the two centers of main girders is about 35 m which is close to the width of two decks. The typical cross sections of the Tanggu Bridge are shown in Fig. 4, which are taken as the third investigated sample for the two-separated paralleled box

3. Description of wind tunnel tests

3.1 Pressure-tapped sectional deck models

The spanwise correlations of the buffeting forces acting on the bridge decks were investigated with pressure synchronous measurement technique via the wind tunnel tests. All pressure measurements were conducted on a serial of motionless sectional deck models that represented the three typical deck geometries of the bridge girders mentioned above. As for the single flat box deck, the sectional model was 2.5 m in length with a length scale of 1:70 (see Fig. 5(a)). There were 67 pressure taps installed on the surface of the bridge deck and distributed uniformly in each section of the sectional model, and there were 469 pressure taps in the whole model in total.

The central portion of the model, which was 0.487 m

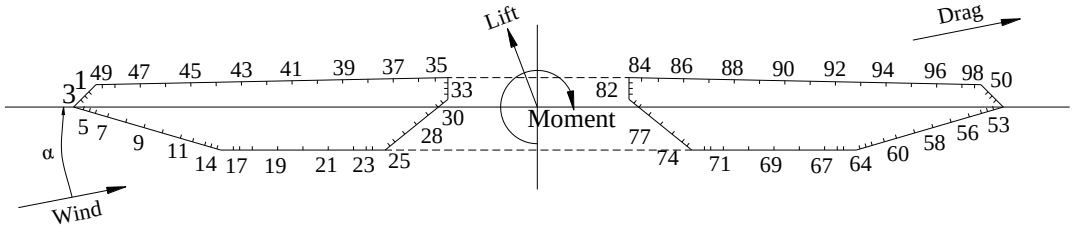

(a) Position and number of pressure-taps

(b) Distribution of pressure-tapped strips

Fig. 6 Pressure strips and taps on the central slotted box girder (Unit: mm)

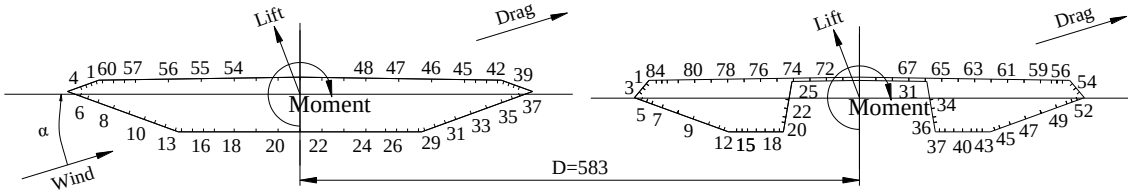

(a) Position and number of pressure-taps

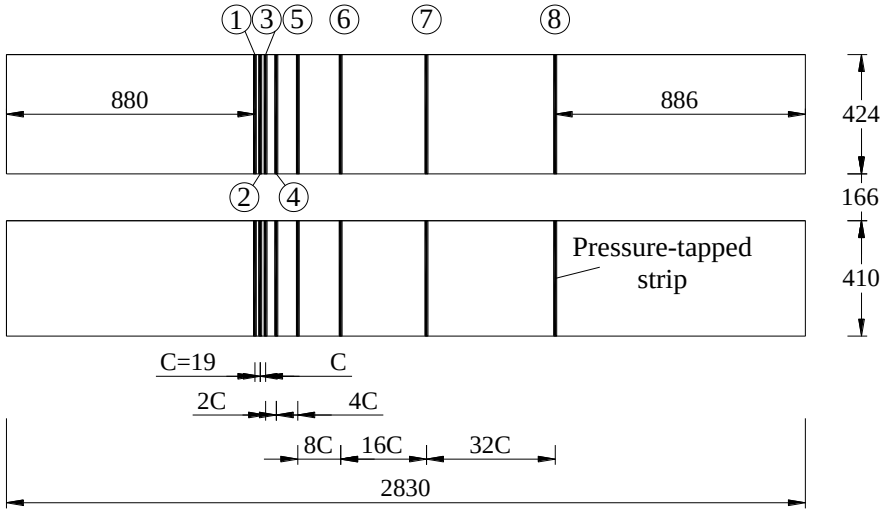

(b) Distribution of pressure-tapped strips

Fig. 7 Pressure strips and taps on the two-separated paralleled box girder (Unit: mm)

away from both end plates of the sectional model on each side, was installed with seven pressure-tapped strips in order to measure time-histories of the surface pressures acting on the deck. The distribution of the pressure-tapped strips on the sectional deck model is depicted in Fig. 5(b). The strips were spaced at 1/8, 1/4, 1/2, 1/2, 1/2 and 1 times the chord length of the box, which was 0.531 m. In all, there were 12 kinds of representative distances considered in the test, namely, 1/8, 2/8, 3/8, 4/8, 6/8, 7/8, 8/8, 10/8, 12/8, 16/8, 20/8, and 23/8 times the chord length of the box.

Fig. 6 shows the position of the pressure taps and the distribution of the pressure-tapped strips for the central slotted box deck model. This motionless sectional model was 2.872 m in length with a length scale of 1:70. There

(a) Open ocean fetch (T.I. =6%)

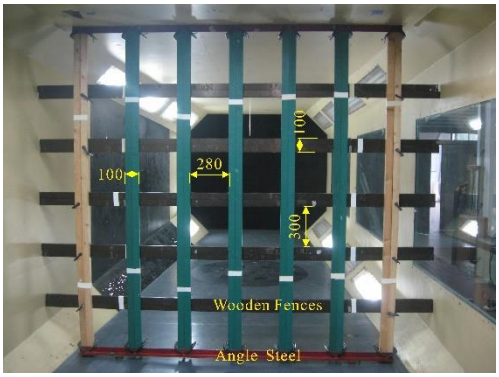

(b) Inshore or lakeshore fetch (T.I. =10%)

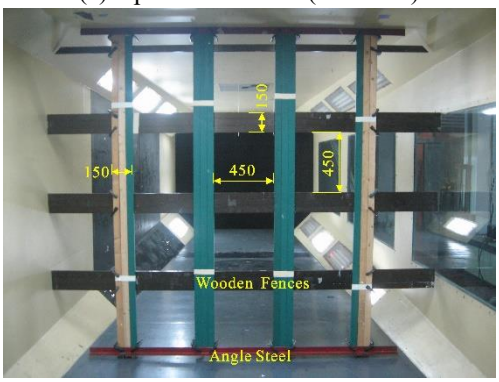

(c) Rural or suburb area (T.I. =15%)

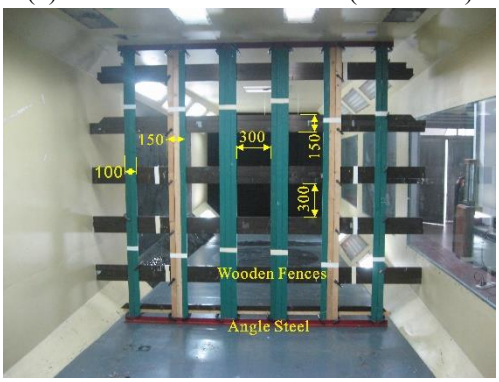

(d) Urban or downtown area (T.I.=20%)

Fig. 8 Wind tunnel simulation of turbulent fields (Unit: mm)

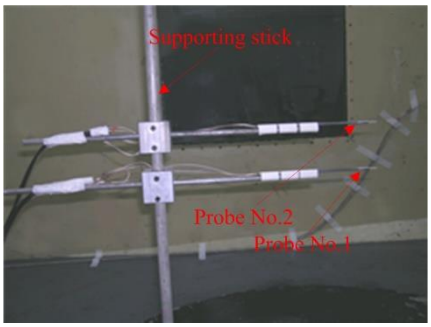

(a) Testing along the Z direction

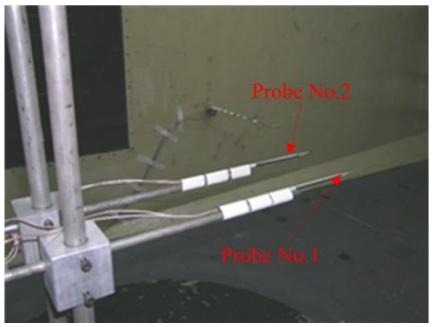

(b) Testing along the Y direction

Fig. 9 Spanwise coherence measurements of incoming turbulent winds in TJ-2

were 49 pressure taps in the windward portion and another 49 pressure taps in the leeward portion in every section of the sectional deck model. In order to measure the surface pressure precisely, more pressure taps were disposed at the corner of the box (see Fig. 6(a)). The central portion of the model, which was 0.379 m away from both end plates of the sectional model, was installed with seven pressure-tapped strips. In the same way as the single flat box sectional deck model, the strips were spaced at 1/8, 1/4, 1/2, 1/2, 1/2 and 1 times the chord length of the box, which is 0.735 m. Therefore, there were also 12 kinds of typical distances considered in the test, which were the same as those of the single flat box sectional deck model.

Fig. 7 shows the position of the pressure taps and the distribution of the pressure-tapped strips for the two-separated paralleled box deck model. This sectional model was composed of a full-closed box and a semi-closed box, both of which were 2.830 m in length with a length scale of 1:60. There were 60 pressure taps in every section of the full-closed box model and 84 taps in every section of the semi-closed box model. The details of the pressure tap distribution can be found in Fig. 7(a). The distance between the central of the windward and leeward boxes was kept at 0.583 m. The central portion of the model, 0.880 m away from the left end plate of the model and 0.886m away from another side, was 1.064 m in length and 8 pressure-tapped strips were installed in that portion. The strips were spaced at intervals of 1, 1, 2, 4, 8, 16, and 24 times characteristic width. It is usually considered that the correlation coefficient of buffeting forces equals to 1 when the distance is less than the integral length scale of the wind turbulence. According to this, the spanwise distance between two nearest pressure-tapped strips was designed as small as possible. In this test, the smallest spanwise distance was

Table 1 Distances between two hotwire probes and wind tunnel walls (Unit: cm)

Between two probes	10	15	20	30	40	50	100
To the bottom wall	58.6	53.6	48.6	98.6	108.6	118.6	168.6
To the side wall	55.5	50.5	45.5	95.5	105.5	115.5	165.5

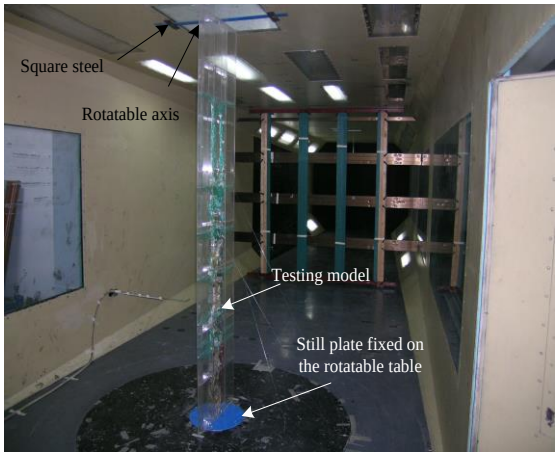

(a) Model for the single flat box deck

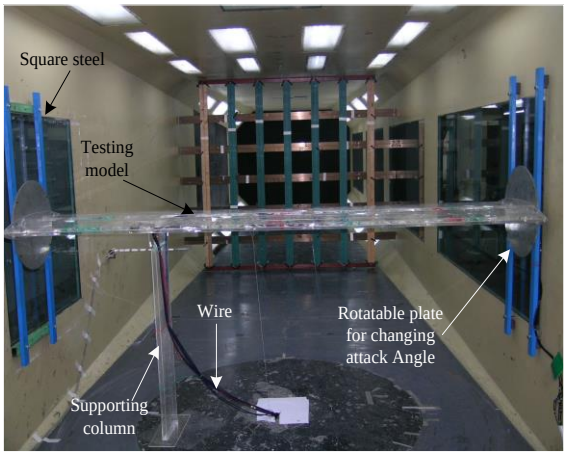

(b) Model for the central slotted box deck

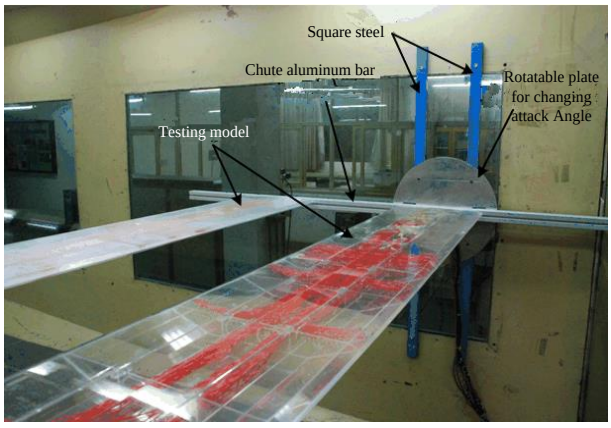

(c) Models for the two-separated paralleled box deck

Fig. 10 Sectional deck models in TJ-2 wind tunnel

0.019 m in which two strips could be installed and selected as the characteristic width. Therefore, there were 14 kinds of separated distances considered in the test, which were 1, 2, 3, 4, 6, 7, 8, 12, 14, 16, 24, 40, 48, and 56 times characteristic width.

3.2 Simulation of turbulence wind field

Turbulent wind flow fields were simulated with horizontal and vertical wood fences at 4.2 m upstream of the model (see Fig. 8). Four uniform turbulent flow fields were simulated, and they represented the four sites at which the real bridge could be located. The target values of the turbulence intensities (T.I.) were calculated according to atmospheric boundary layer at the heights of 50-70 m. The field with a T.I. of 6% represents an open ocean fetch, the field with a T.I. of 10% represents an inshore or lakeshore fetch, the field with a T.I. of 15% represents a rural or suburb area and the field with a T.I. of 20% represents a crowded downtown area. More details of the simulated turbulent fields are summarized in Section 5.1.

3.3 The measurement setup of incoming turbulent winds

The spanwise correlation measurements of incoming turbulent winds were conducted by the 2D Streamline Hotwire system which is produced by DANTEC company, Denmark. Two separate 2D hotwire probes, which can be used to measure the wind speed components of u and v or u and w at one record, were employed to measure the wind speeds of two positions simultaneously. Probe No.1 was fixed at a constant position in a test and probe No.2 changed its positions in each measurement and kept different distances to the fixed probe No.1.

The distances between two probes during the wind tunnel tests were illustrated in Table 1. Considering that the models of wind pressure tests might be vertically and horizontally installed in different cases, the wind speeds of vertical and horizontal profiles were investigated separately. While testing the vertical profile, probe No.1 was at the position, with a height of 68.8 cm to the wind tunnel bottom and a distance of 150 cm to one side wall of the wind

tunnel, and probe No.2 had the same coordinates at X and Y axes as those of the fixed probes. While testing the horizontal profile, probe No.1 was at the position, with a height of 125 cm to the wind tunnel bottom and a distance of 65.5 cm to one side wall, and the probe No.2 had the same coordinates at X and Z axes as those of the fixed probes. The experimental data of incoming wind speeds had a sample length of 34,816, and a sampling frequency of 400 Hz. The setup of two hotwire probes in the wind tunnel are depicted in Fig. 9.

3.4 Information of wind tunnel tests

Fig. 10 shows the pressure-tapped sectional model mounted in TJ-2 wind tunnel in Tongji University and the location of the Pitot tube and cobra probe that were used to calibrate the mean wind speed and record the transient 3D turbulences, respectively. Two metal fixation systems were used to mount the sectional model. One system mounted the sectional model vertically which was used for the wind tunnel test of the single flat box deck (see Fig. 10(a)). The bottom end of the model was connected to a circle steel plate that was fixed on the rotatable plate to change the angle of wind attack. A rotatable steel axis and square steel were installed in the top end of the model. Therefore, the model can rotate but not move.

Another metal fixation system mounted the sectional model horizontally. This system was used for the wind tunnel test of the central slotted box deck and the two-separated paralleled box deck (see Fig. 10(b) and 10(c)). Two aluminum plates were fixed at the two ends of the sectional model and allowed to rotate by fixing different screws to the square steel. All the models were further stabilized with guy wires to avoid vibration.

Pressure tests were conducted in four types of turbulent wind flow fields at two wind speeds of 8 and 12 m/s with -3°,0°, and 3°wind attack angles. Additional tests were conducted in a smooth flow field at wind speed of 12 m/s with -3°,0°and 3°wind attack angles. The time-histories of the aerodynamic pressures from the pressure-taps were acquired and collated simultaneously. The time-histories of the buffeting forces were obtained by integration of the aerodynamic pressures. The time-histories of 3D wind speeds were also simultaneously recorded by the cobra probes along with the pressure measurements.

4. Aerodynamic force on a bridge deck

4.1 Formulation of the quasi-steady aerodynamic force

In the pressure tests, the pressure on the surface of bridge deck was measured through the pressure-taps. Therefore, the aerodynamic force can be obtained from the integration of wind pressure. The aerodynamic force per unit length can be calculated as the integration of the distributed aerodynamic pressures on a pressure-tapped strip as

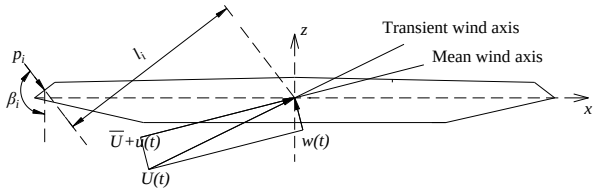

Fig. 11 Wind axes and pressures on the section outline

$$F_{L,b}(t)=\sum_{i=1}^{N} p_i(t)\times\delta_i\times\cos(\beta_i+\alpha) \tag{1}$$

$$F_{D,b}(t)=\sum_{i=1}^{N} p_i(t)\times\delta_i\times\sin(\beta_i+\alpha) \tag{2}$$

$$F_{M,b}(t)=\sum_{i=1}^{N} p_i(t)\times\delta_i\times l_i^2 \tag{3}$$

where $Fk,b(t)$ (k=L, D, and M) are the time-histories of the aerodynamic lift force, aerodynamic drag force, and aerodynamic lift moment, respectively. $p_i(t)$ is the time-history of the wind pressure on the i^{th} surface point of the bridge deck. δ_i is the characteristic length on the deck section outline for the aerodynamic pressure p_i. β_i is the angle between pressure and the vertical structural axis z (see Fig. 11). α is the wind attack angle of incidence. l_i is the distance between the i^{th} surface point and the center of the bridge deck, and N is the total number of wind pressure points on the section where the pressures are measured.

4.2 Spanwise coherence function

The auto-spectrum of aerodynamic forces can be obtained based on Eqs. (1)-(3) through Fourier transformation. According to the theory of stochastic vibration, spanwise coherence function of aerodynamic forces can be defined and calculated as

$$R_{\alpha_1\alpha_2}=\frac{\left|S^{cr}_{\alpha_1\alpha_2}(K_\Delta)\right|}{\sqrt{S_{\alpha_1}(K_\Delta)S_{\alpha_2}(K_\Delta)}} \tag{4}$$

where $R_{\alpha_1\alpha_2}$ is the root coherence function of the aerodynamic forces. α_1 and α_2 are either the aerodynamic forces acting on the two sections of the bridge deck or the wind turbulence components at the two locations in the wind field. $K_\Delta=f\Delta/U$ is the reduced frequency with respect to the spanwise distance between two sections of the bridge deck or two locations. S_{α_1} and S_{α_2} are the auto-spectrum of α_1 and α_2, respectively. $S^{cr}_{\alpha_1\alpha_2}$ is the cross-spectrum between α_1 and α_2, which can be calculated as

$$S^{cr}_{\alpha_1\alpha_2}(K_\Delta)=S^{C}_{\alpha_1\alpha_2}(K_\Delta)+iS^{Q}_{\alpha_1\alpha_2}(K_\Delta) \tag{5}$$

where $S^{C}_{\alpha_1\alpha_2}$ is the co-spectrum of α_1 and α_2, $S^{Q}_{\alpha_1\alpha_2}$ is the orthogonal spectrum of α_1 and α_2, and i is the symbol of imaginary unit, defined as $i^2=-1$.

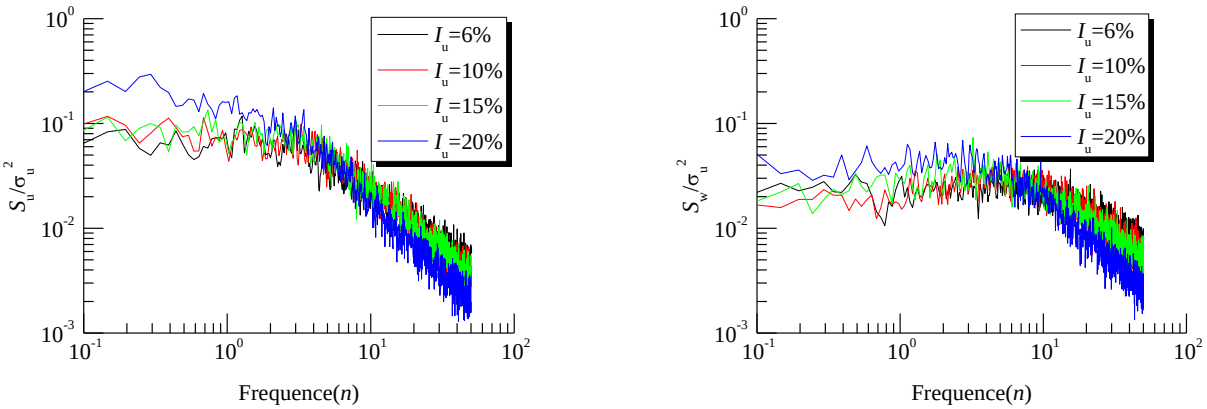

(a) Spectra of u (b) Spectra of w

Fig. 12 Dimensionless auto-spectra of the turbulent components u and w

Table 2 Measured turbulence intensities and integral length scales

Turbulence Intensity	L_{ux}	L_{vx}	L_{wx}	L_{uy}	L_{vy}	L_{wy}	L_{uz}	L_{vz}	L_{wz}
6%	0.138	0.047	0.047	0.066	0.085	0.055	0.078	0.044	0.080
10%	0.167	0.063	0.059	0.084	0.099	0.068	0.088	0.066	0.102
15%	0.214	0.086	0.079	0.117	0.110	0.088	0.103	0.070	0.107
20%	0.511	0.127	0.153	0.185	0.132	0.139	0.167	0.119	0.189

5. Results and discussions

5.1 Characteristics of the simulated turbulent field

The measured turbulence intensity of the four simulated turbulent flow fields is defined as

$$I_u = \frac{\sigma_u}{\overline{U}};\ I_w = \frac{\sigma_w}{\overline{U}} \tag{6}$$

where σ_u and σ_w are the standard deviations of u and w, respectively. $\overline{U}$ is the mean wind speed.

Since the vertical fluctuation is usually more dominant in the buffeting response, the turbulence intensities mentioned below are the vertical turbulence intensities. The measured turbulence intensities and the integral length scales are listed in Fig. 12 and Table 2. Based on Taylor's hypothesis which states that the vortex patterns do not change as wind sweeps them leeward, the integral length scales can be estimated as follows:

$$L_\alpha^r = \overline{U}\int_0^\infty Cov_\alpha(\tau)\cdot d\tau / \sigma_\alpha^2 \tag{7}$$

where L_α^r is the integral length scale and r denotes the x, y, or z and α denotes the turbulent component such as u, v or w. x, y and z represent the downwind (parallel to wind tunnel axis), horizontal crosswind and vertical directions, respectively, and u and w represent the downwind and vertical fluctuating velocities of the turbulence wind, respectively. $Cov_\alpha(\tau)$ is the covariance of the turbulent components α_1 and α_2 in the direction of r.

Fig. 12 shows the dimensionless auto-spectra of the turbulent components u and w in different turbulent flow fields. It can be found that the four turbulent flow fields had a similar distribution of dimensionless auto-spectra and the energy of turbulence were mainly concentrated in the low frequency range.

5.2 Correlation comparison between the buffeting force and the incident wind turbulence

Fig. 13 shows the measured spanwise root coherence of the drag force (D), lift force (L), and torsional moment (M) on the three typical bridge decks. The measured spanwise root coherence functions of the fluctuating components u and w are also plotted in the figures together with the calculation of an empirical formula suggested by Davenport, $R = e^{-7K}$, where K is a kind of reduced frequency. Fig. 13(a) gives an example of the measured spanwise root coherence of the single flat box deck at wind speed of 12 m/s, with a wind attack angle of 0°, under a turbulent wind flow field with a T.I. of 10%. For this example, the characteristic distance of the buffeting force is 133 mm and the characteristic distances of the fluctuating components u and w are 100 mm. As shown in the figure, the result of the drag force was larger than the results of the fluctuating components u and w in most of the reduced frequency range except in the range of $0.15 \le K_\Delta \le 0.3$. The result of the empirical formula could not match well with that of drag force in the whole reduced frequency range. In addition, while the reduced frequency was larger than 0.3, the results varies dramatically which may be the effect of signature turbulence. The measured spanwise root coherence of the lift force and the torsional moment, also shown in Fig. 13(a), were remarkably larger than those of the components u and w in the entire reduced frequency range and the results of the empirical formula in most of the reduced frequency range. It is worthwhile that except the

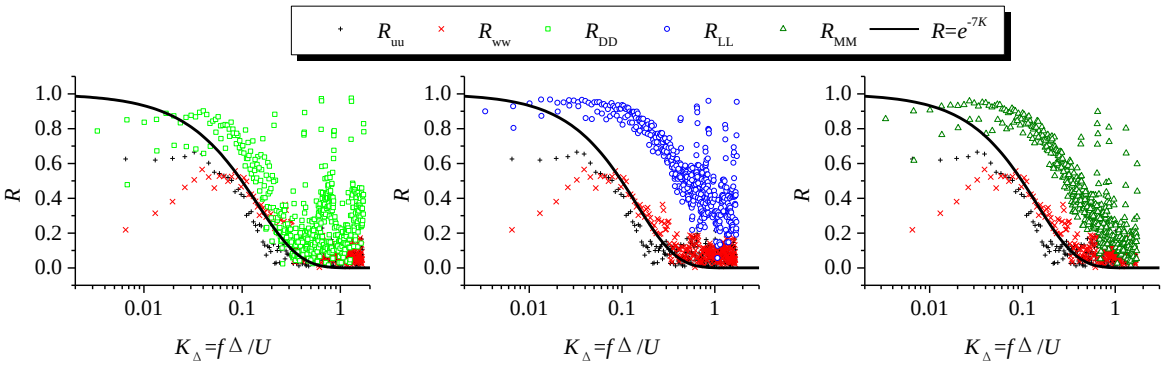

(a) Results for the single flat box deck

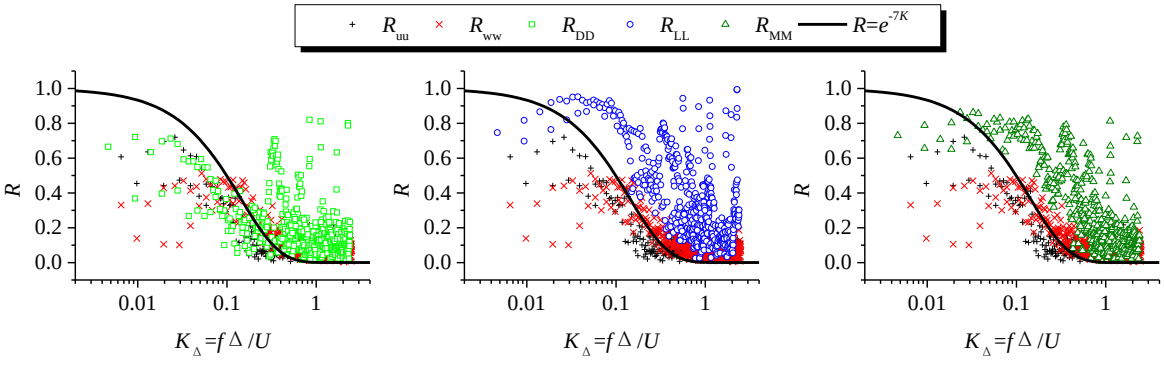

(b) Results for the central slotted box deck

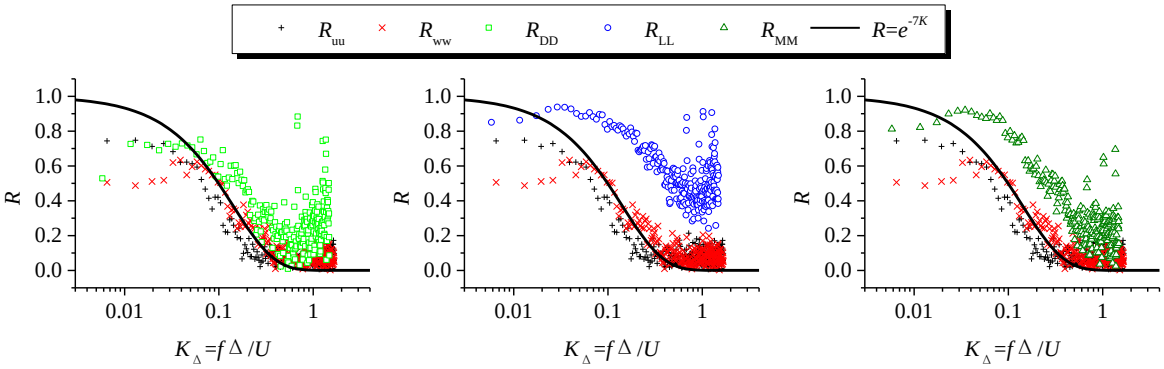

(c) Results for the full-closed box on the windward side of the two-separated paralleled box deck

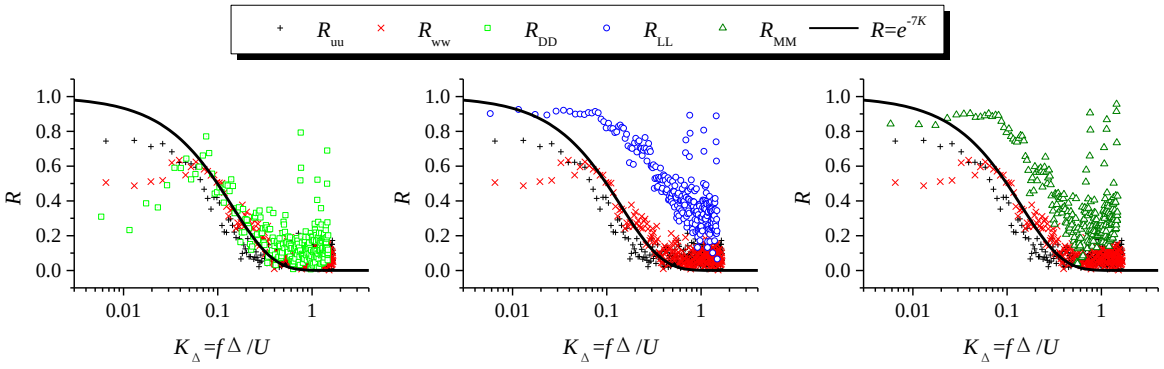

(d) Results for the semi-closed box on the leeward side of the two-separated paralleled box deck

Fig. 13 Examples of spanwise root coherence between the buffeting force and turbulent components *u* and *w*

reduced frequency range of $0.1 \le K_\Delta \le 0.4$, the calculation of empirical formula has an obvious difference with the results of the components u and w, not to mention those of buffeting forces. It is meant that the spanwise coherence of wind turbulence can instead of that of drag force just in the small range of the reduced frequency. Except for the circumstances mentioned above, the measured spanwise root coherences of the single flat box deck are clearly stronger than those of the fluctuating components u and w, and the empirical formula is not applicable.

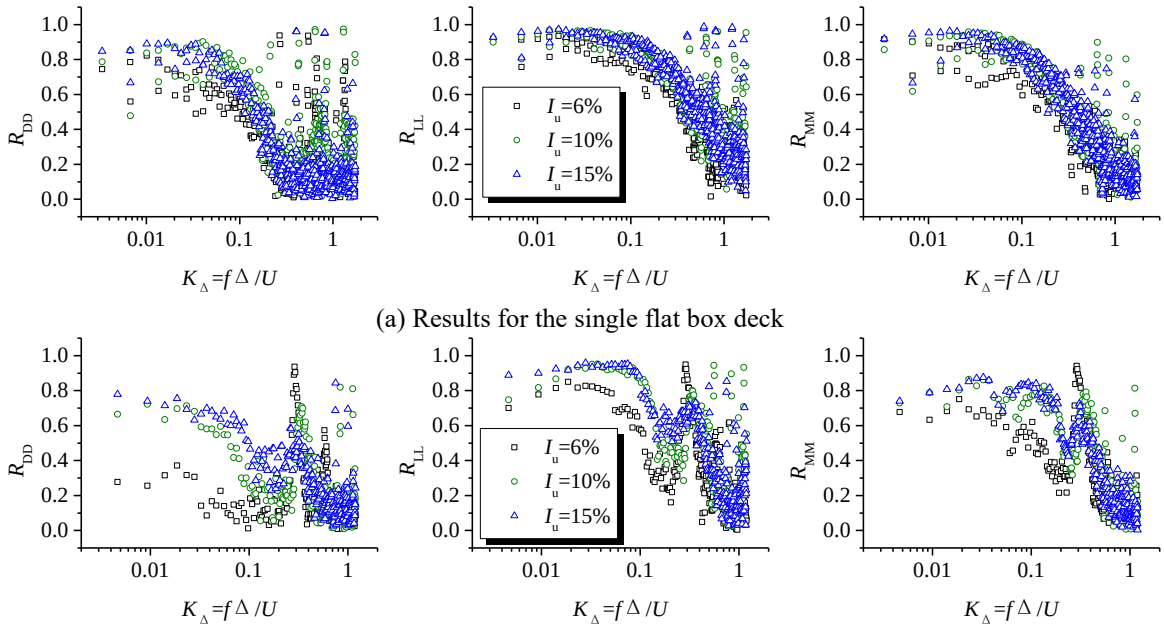

(a) Results for the single flat box deck

(b) Results for the central slotted box deck

Fig. 14 Examples of spanwise root coherence under different turbulence intensity wind fields

Figs. 13(b) depicts an example of measured spanwise root coherence of the central slotted box deck at wind speed of 12 m/s, with a wind attack angle of 0°, under a turbulent wind flow field with a T.I. of 10%. For this example, the characteristic distance of the buffeting force is 92 mm and the characteristic distances of fluctuating components *u* and *w* are 100 mm. As shown in the figure, the result of the drag force was close to the results of the fluctuating components u in the low reduced frequency range, while the reduced frequency was larger than 0.2, the result of the drag force varied dramatically and was clearly larger than those of the fluctuating components u. Compared with the results of fluctuating components w, the results of drag force was remarkably larger except for the reduced frequency range of $0.06 \le K_\Delta \le 0.2$, which was slightly larger than the former. Additionally, the calculation of empirical formula was larger when the reduced frequency was smaller than 0.2, while the results of drag force was larger in the rest of reduced frequency range. Furthermore, the measured spanwise root coherence of the lift force and the torsional moment acting on the central slotted box deck were predominant larger than those of the fluctuating components u and w in the entire reduced frequency range, the characteristics of which were similar to those of the single flat box deck.

Fig. 13(c) and 13(d) shows the examples of the measured spanwise root coherences of the two-separated paralleled box deck at wind speed of 12 m/s, with a wind attack angle of 0°, under a turbulent wind flow field with a T.I. of 10%. Where the characteristic distance of buffeting force is 114 mm and the characteristic distances of the fluctuating components *u* and *w* are 100 mm. Fig. 13(c) depicts the results of the full-closed box deck on the windward side and Fig. 13(d) that of the semi-closed box deck on the leeward side. As is shown in the figure, when the reduced frequency was larger than 0.04, the results of drag force were slightly larger than those of the components u and w. As for the full-closed box deck, the result of drag force approached that of the fluctuating components u but was clearly larger than that of the fluctuating components w, while for the semi-closed box deck, the result of drag force was significant smaller than those of the fluctuating components *u* and *w*. What's more, the results of the lift force and the torsional moment were remarkable larger than those of the fluctuating components *u* and *w* in the entire reduced frequency range, which is similar to the results of other typical bridge decks.

Therefore, it can be concluded that the spanwise coherences of buffeting forces were markedly stronger than the spanwise coherences of the wind turbulences. In addition, the empirical formula suggested by Davenport cannot express the spanwise coherence of the buffeting forces very well.

5.3 Influence of the wind turbulence intensity

Fig. 14 shows the examples of the measured spanwise root coherence of the buffeting forces acting on the typical bridge decks in the different turbulent wind flow fields. The results of the single flat box deck with a wind attack angle of 0°, at the wind speed of 12 m/s, in the turbulent wind flow fields with T.I.s of 6%, 10% and 15% are depicted in Fig. 14(a). As shown in the figure, the measured spanwise root coherences of the buffeting forces with a T.I. of 15% are slightly bigger than those with a T.I. of 6% but almost equal to those with a T.I. of 10% in almost entire reduced frequency range. This indicates that the turbulence intensity had little effect on the spanwise coherence of the buffeting forces on the single flat box deck.

Fig. 14(b) gives the measured results of the central slotted box deck at the wind speed of 12 m/s, with a wind

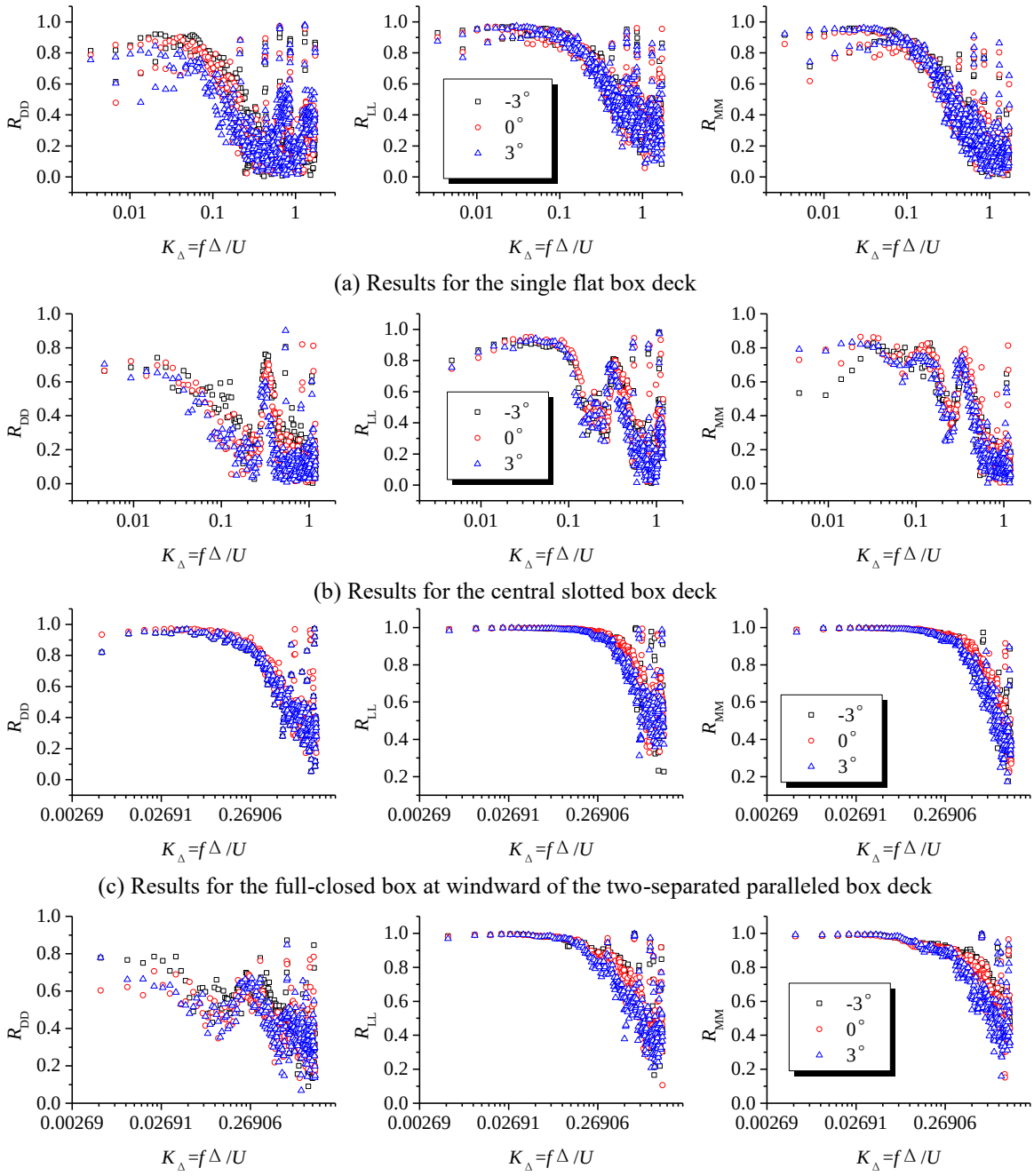

(a) Results for the single flat box deck

(b) Results for the central slotted box deck

(c) Results for the full-closed box at windward of the two-separated paralleled box deck

(d) Results for the semi-closed box leeward of the two-separated paralleled box deck

Fig. 15 Examples of spanwise root coherences under different wind attack angles

attack angle of 0°, in the wind flow field with T.I.s of 6%, 10% and 15%. As shown in the figure, the measured spanwise root coherences with a T.I. of 6% are distinct smaller than the measured spanwise root coherences with a T.I. of 15% in the reduced frequency range from 0.0 to 0.2. The results in the turbulent wind flow field with a T.I. of 10% lay between the results with a T.I. of 6% and the results with a T.I. of 15%. In addition, the results in the turbulent wind flow field with different T.I.s in the rest of reduced frequency range nearly overlapped. It is worth noting that unlike the results of a single flat box deck, the measured spanwise root coherence functions of the buffeting forces involved some notable peaks that might be induced by the signature turbulence, which could be named as the signature turbulence effect and appeared in the reduced frequency range from 0.2 to 0.35. Moreover, the results in the wind flow field with a T.I. of 6% is much larger than the results with T.I.s of 10% or 15% and the peak value reached up to 1.0 in the predominant reduced frequency. This was mainly because the high turbulence intensity may transfer the energy at the predominant reduced frequency induced by the signature turbulence to the lower or higher reduced frequency zone.

It can be concluded that the turbulence intensity had little effect on the spanwise coherences of the buffeting forces acting on the deck without the signature turbulence effect, as shown as the results of the single flat box deck.

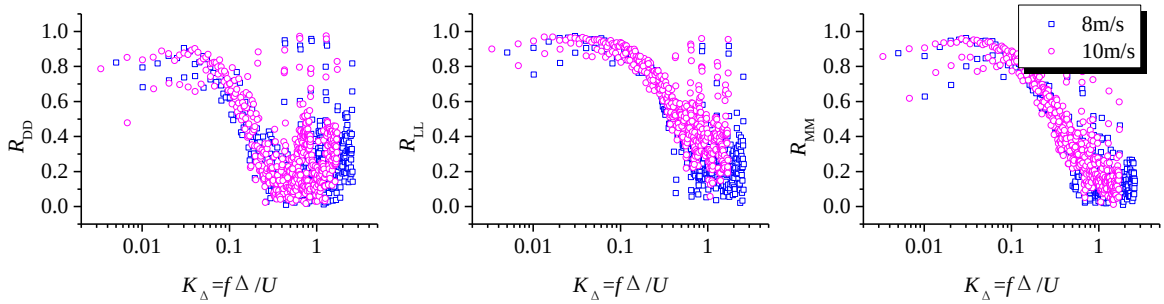

Fig. 16 Spanwise root coherences under different wind speeds

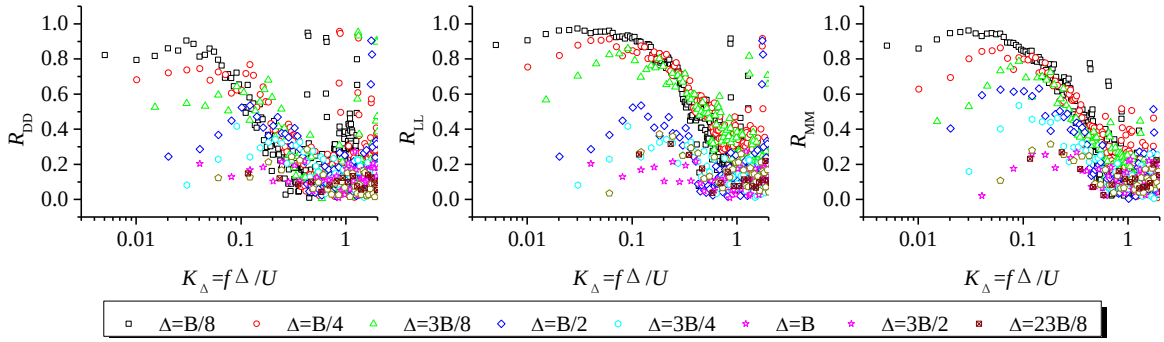

(a) Results for the single flat box deck

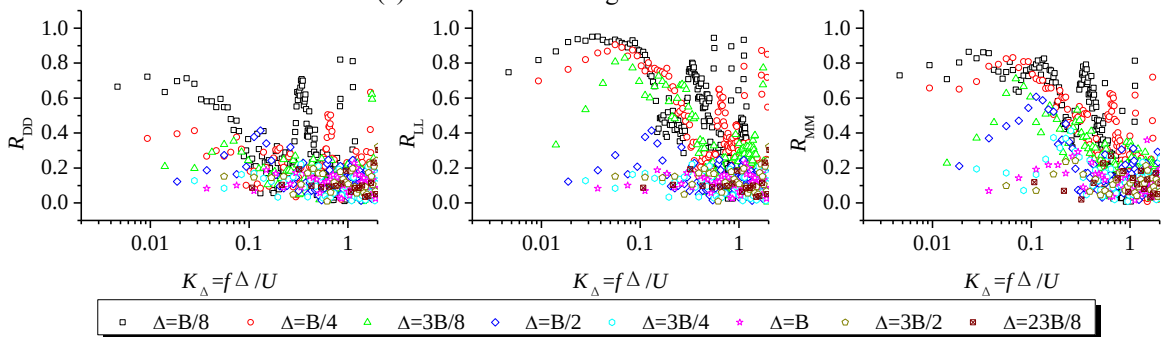

(b) Results for the central slotted box deck

Fig. 17 Examples of spanwise root coherences with different characteristic distances

However, with the signature turbulence effect, the spanwise coherences in the turbulent wind flow fields with different turbulent intensities had marked differences, especially in the low reduced frequency zone.

5.4 Influence of the wind attack angle

Fig. 15 gives the examples of the measured spanwise root coherences of buffeting forces acting on typical bridge decks under different attack angles. The measured results of the single flat box deck and the central slotted box deck were all conducted at a wind speed of 12 m/s, in the turbulent wind flow field with a T.I. of 10% and are shown in Fig. 15(a) and 15(b), respectively. The measured results of the two-separated paralleled box deck were obtained at a wind speed of 12 m/s, in the turbulent wind flow field with a T.I. of 15% and are given in Figs. 15(c) and 15(d), where the full-closed box is on the windward side and the semi-closed box is on the leeward side. As shown in the figure, although there is some minor diversity, the spanwise root coherences under different wind attack angles almost approach to each other. It is indicated that the wind attack angle has only a slight effect on the spanwise coherence of the buffeting forces acting on the typical bridge deck.

5.5 Influence of the wind speed

Fig. 16 gives an example of spanwise root coherences of the buffeting forces acting on the single flat box deck at the wind speed of 8 m/s and 12 m/s. As the figure shows, the measured results at a wind speed of 8 m/s were almost overlapped by the results at a wind speed of 12 m/s in the entire reduced frequency zone. In other words, as long as the wind speeds do not vary dramatically, the spanwise coherences of the buffeting forces are almost equal to each other. In fact, the same conclusion can be obtained from the measured results of the central slotted box deck and the two-separated paralleled box deck.

5.6 Influence of the distance between testing sections

Fig. 17 shows the examples of the measured spanwise

root coherence of the buffeting forces acting on the single flat box deck (see Fig. 17(a)) and the central slotted box deck (see Fig. 17(b)) with different characteristic distances. In this picture, all the measured results were obtained at a wind speed of 12 m/s, with a wind attack angle of 0°, in the turbulent wind flow field with a T.I. of 10%. As shown in the figure, the spanwise root coherences varied with the increase of the reduced frequency and the coherence values at the same reduced frequency but with the different characteristic distance, are quite different. It can be seen that at the range of low reduced frequency ($0.0 < K_{\Delta} < 0.8$), the measured spanwise root coherences were sensitive in respect to the characteristic distance. The smaller the distance was, the better the coherences were, and vice versa. Additionally, the attenuation of the coherences with the small characteristic distances (such as $\Delta = B/8$, $\Delta = B/4$, or $\Delta = 3B/8$ in Fig. 17(a)) was much faster than the attenuation of the coherences with the large characteristic distances in the reduced frequency range from 0.0 to 0.4. Moreover, it can be seen that at the range of the high reduced frequency ($K_{\Delta} > 0.8$), the measured spanwise root coherences varied around 0.2 with the different characteristic distances, except for some coherence peaks due to the signature turbulence effect.

As shown in Fig. 17(b), the measured spanwise root coherences had some predominant peaks, especially in the R_{LL} and R_{MM}. These coherence peaks appeared while the characteristic distances were less than $B/2$. When the characteristic distance was larger than $B/2$, the spanwise root coherences decreased to around 0.15. This indicated that for the blunt bridge deck, the spanwise coherence was remarkably influenced by the signature turbulence effect, especially for the small distance between sections. In summary, the spanwise coherences with the different characteristic distances had an obvious difference at the same reduced frequency zone, and they were greatly affected by the signature turbulence effect at the small distance between sections

6. New empirical model of the spanwise root coherence functions

6.1 Characteristics of the spanwise root coherence functions

In Section 5, some examples were depicted in Figs. 13-17 and the possible influence factors were discussed. It can be concluded that the spanwise coherence is slightly affected by the wind speed and the wind attack angle. Therefore, the spanwise coherence of typical bridge decks can be investigated via a wind pressure tunnel test with a wind attack angle of 0° at a certain wind speed. The turbulence intensity has some effect on the spanwise coherence, especially for the blunt bridge deck such as the central slotted box deck. The wind tunnel pressure test should be conducted in the turbulent wind flow field with the given turbulence intensity with respect to the real bridge site. In addition, the characteristic distances between bridge sections have a great influence on the spanwise coherences of the typical bridge decks. As shown in the Figs. 13-17, the spanwise coherences often involve high frequency peaks due to the signature turbulence. Additionally, it can be found that the coherence peaks induced by the signature turbulence have different predominant reduced frequency, while the reduced frequency is expressed with the characteristic distance Δ. The distribution of coherence peaks presents a disordered law. Therefore, this paper has attempted to introduce a new viable to express the spanwise coherence and explain the rule of the signature turbulence effect.

The signature turbulence induced by the flow around the bridge deck has some intrinsic relationship with the characteristic length of bridge breadth. Consequently, in the new empirical model of spanwise root coherence function, the deck-width-related reduced frequency (K_B) was chosen for the first variable. Another variable selected for the coherence function was the reduced distance used to consider the characteristic distance effect, which can be expressed as a dimensionless form as

$$l_{\Delta} = \Delta / L^{y} \tag{8}$$

where $L_y = \sqrt{L_u^y \cdot L_w^y}$ is the average of the integral scales for the turbulence components u and w.

Fig. 18 shows an example of spanwise coherence coefficients of the lift force (R_{LL}) acting on the central slotted box deck at a wind speed of 12 m/s, with a wind attack angle of 0°, and in the turbulent wind flow field with a T.I. of 10%. It is mentioned that the top tick label of Fig. 18 is the deck-width-related reduced frequency (K_B) and the bottom tick label is the distance-related reduced frequency (K_{Δ}). As shown in Fig. 18, it can be found that, (1) R_{LL} gradually decreased with the increasing of l_{Δ} and the falling velocity was decreasing until l_{Δ}>9.67, for which the values of R_{LL} was generally smaller than 0.2. (2) For a determined l_{Δ}, R_{LL} had a markedly decreasing tendency with the reduced frequency approaching zero. In other words, a peak of R_{LL} occurred within a very low frequency zone. Moreover, the peak diminished gradually with the increase of l_{Δ}. (3) Under the influence of the signature turbulence, R_{LL} had several narrow-band peaks in the frequency region of K_B >2, and the peak values could exceed the value at close to zero. (4) With the increase of l_{Δ}, the values of K_B corresponding to the above peaks due to signature turbulent effect remained almost the same whilst the values of K_{Δ} changed. This was because the eminent frequencies of the signature turbulence depended on the shape of deck cross section, and thus they were related to the characteristic length of the deck cross section but independent of the separated distance. In connection with this, the root coherence coefficients of the buffeting forces should be expressed as a function of the deck-width-related reduced frequency (K_B) instead of the distance-related reduced frequency (K_{Δ}). Of course, this also depends on the spanwise separation distance and the spanwise integral length scales of the incident wind turbulence. Therefore, it can be expressed as a two-variable function of K_B and l_{Δ}. (5) With the increase of the separated distance, the drop of

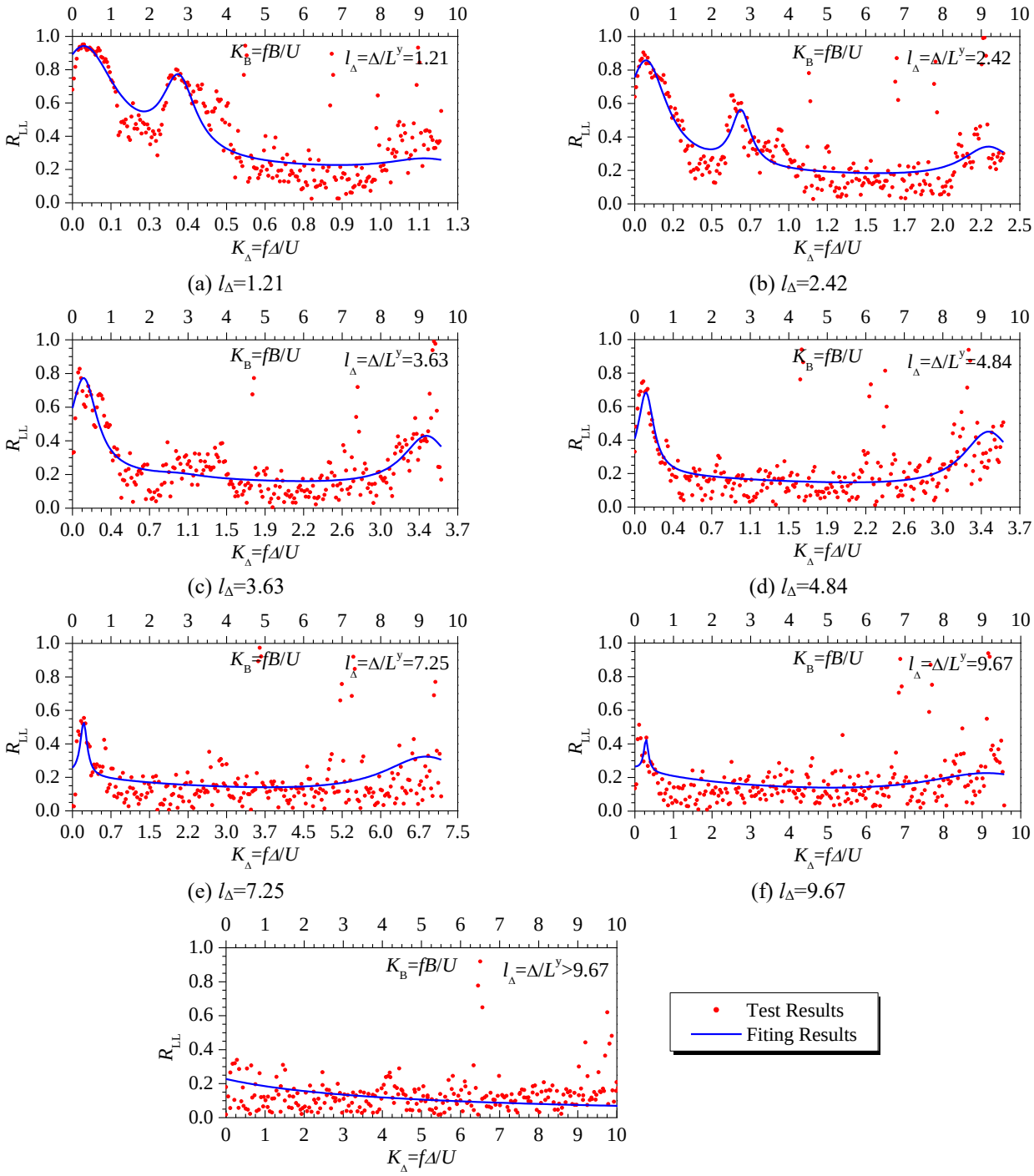

(a) l_Δ=1.21 (b) l_Δ=2.42

(c) l_Δ=3.63 (d) l_Δ=4.84

(e) l_Δ=7.25 (f) l_Δ=9.67

(g) l_Δ>9.67

Fig. 18 Example of the pan-wise root coherence of the central slotted bridge deck

the root coherence peaks at the high-frequency zone due to signature turbulence was not evident or much slower compared to that at the low frequency zone due to the incident wind.

Fig. 19 shows an example of the spanwise coherence coefficients of the drag force (R_{DD}) acting on the semi-closed box leeward of the two-separated paralleled box deck at a wind speed of 12 m/s, with a wind attack angle of 0°, and in the turbulent wind flow field with a T.I. of 10%. It is clear that the spanwise coherence functions of the two-separated paralleled box deck expressed by the new model represent similar characteristics to those of the central slotted box deck. As shown in the figure, the coherence functions have some peaks at the predominant deck-width-related reduced frequencies near 0.08 (see Figs. 19(a), 19(c), 19 and etc.), 1.08 (see Fig. 19(a), 19(c), 19(d)), 4.57 (see Figs. 19(d), 19(j) and 19(l)) and 5.38 (see Fig. 19(k)). However, the predominant distance-related reduced frequencies that these peaks appeared are not equal to each other. This proves that the signature turbulence effect

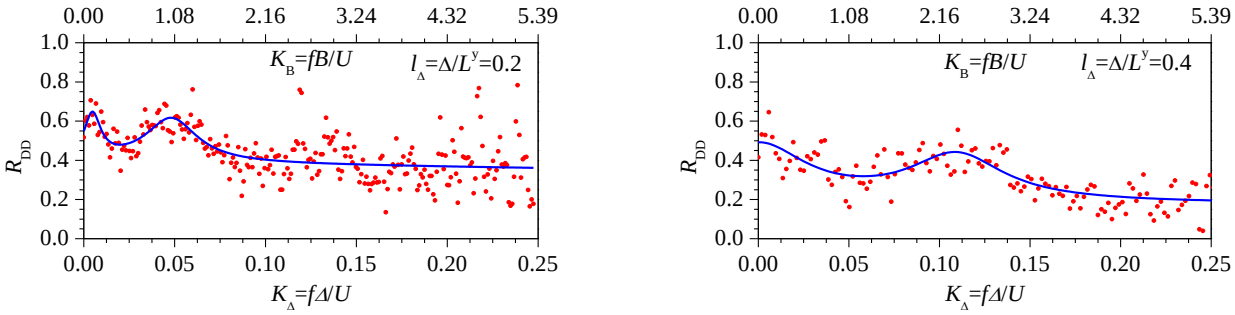

(a) l_Δ=0.2

(b) l_Δ=0.4

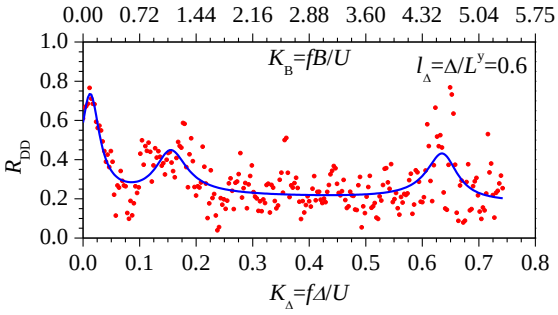

(c) l_Δ=0.6

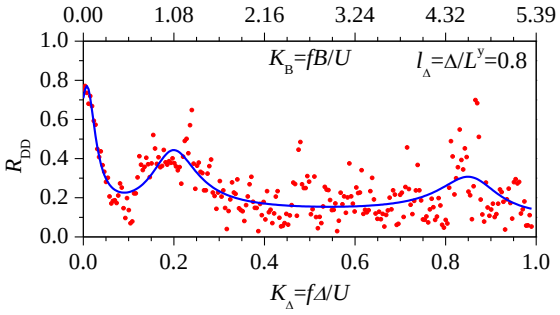

(d) l_Δ=0.8

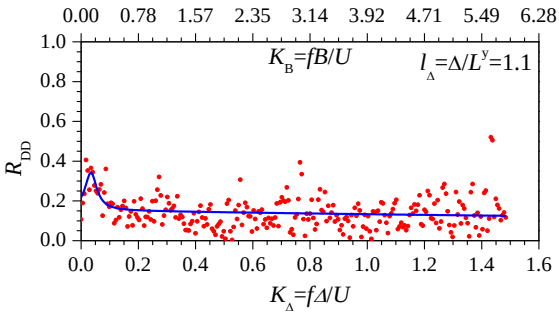

(e) l_Δ=1.1

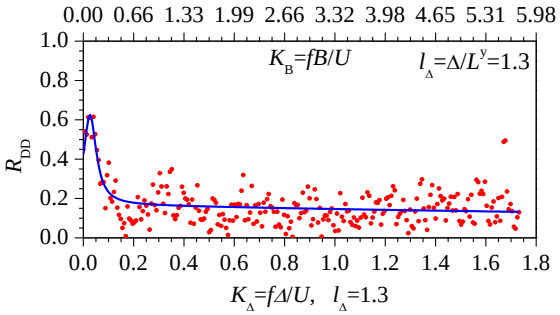

(f) l_Δ=1.3

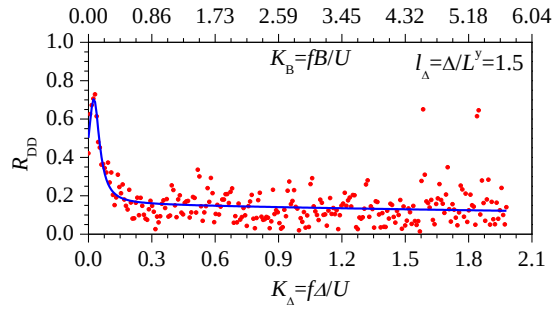

(g) l_Δ=1.5

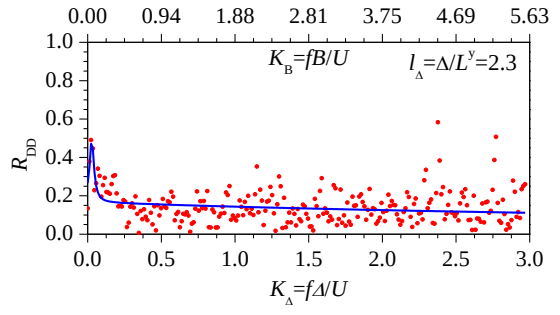

(h) l_Δ=2.3

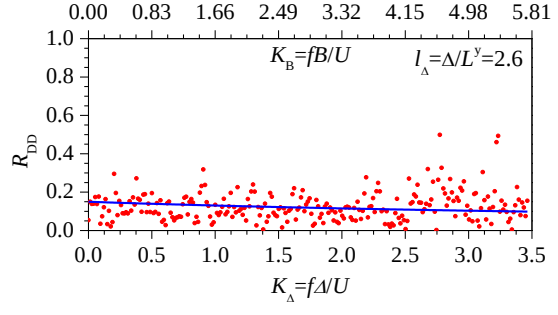

(i) l_Δ=2.6

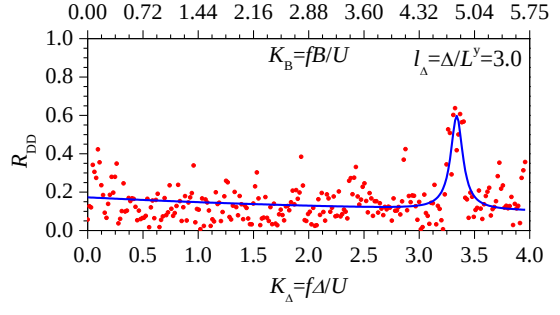

(j) l_Δ=3.0

Fig. 19 Example of the spanwise coherence coefficients of the two-separated paralleled box decks

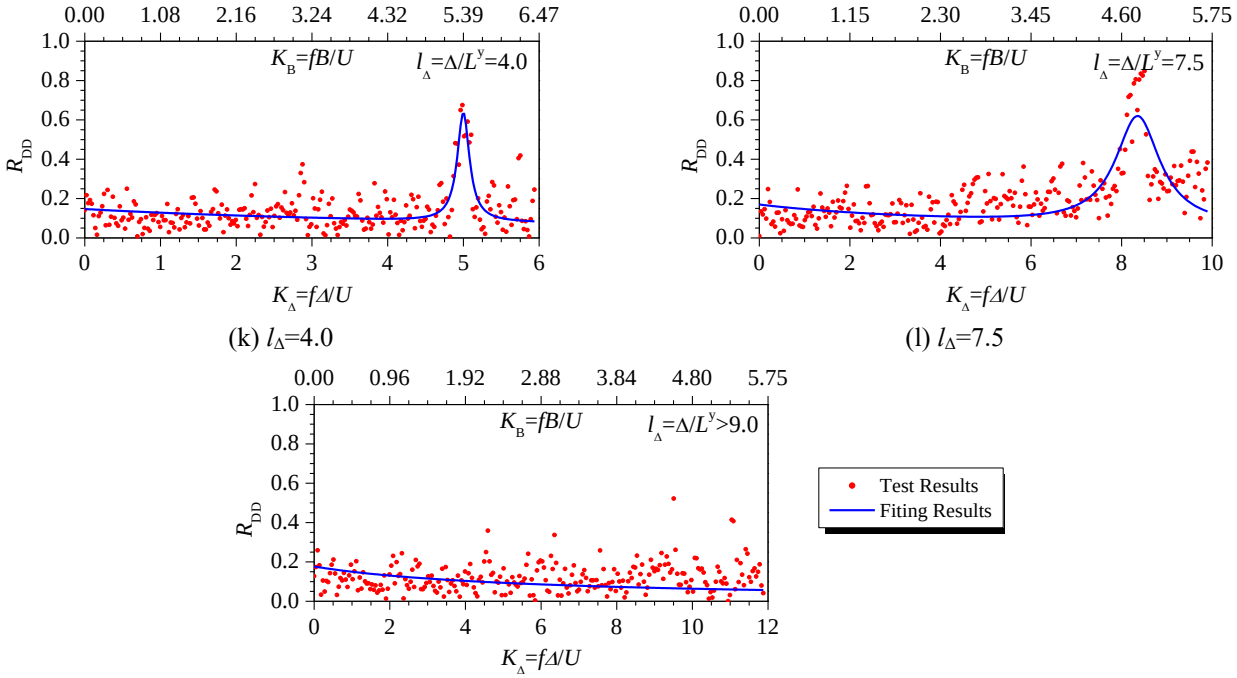

(k) l_Δ=4.0 (l) l_Δ=7.5

(m) l_Δ>9.0

Fig. 19 Continued

is related to the bridge deck breadth and that it cannot be properly reflected by the characteristic distance.

6.2 Fitting of the root coherence functions

Based on the foregoing analysis, the following model of root coherence function expressed with a sum of the rational fractions is then presented to fit the test data, with consideration of the peaks due to both the signature turbulence and the incident wind turbulence.

$$R_{f_1 f_2}(K_B) = \frac{1}{p_1[K_B - p_2]^2 + p_3} + \frac{1}{K_B + p_4} + \sum_{i=1}^{n} \frac{1}{p_{5i}[K_B - p_{6i}]^2 + p_{7i}} \quad (9)$$

where the first two rational fractions are used to reflect the contribution of the incident wind turbulence, while the rest of the rational fractions are used to reflect the contribution of the signature turbulence. n is the number of the peaks due to the signature turbulence, which is included. i represent the i^{th} peak zone, and p_1-p_4 and p_{5i}-p_{7i} are the parameters to be fitted for every value of l_Δ, these parameters thus vary with l_Δ.

The fitted curves of R_{LL} of the central slotted bridge deck for various spanwise reduced distances are also plotted in Fig. 18. The fitted curves of R_{DD} for the semi-closed box on the leeward side from the two-separated paralleled box deck are also plotted in Fig. 19. One can find from these figures, the proposed rational fraction model of the root coherence function has a good fitting effect. It should be pointed out that it is only necessary to include a few root coherence peaks within relatively low frequency region for the buffeting analysis because long span bridges normally have very low fundamental natural frequencies. Thus, their buffeting responses are often contributed by the low frequency components of buffeting forces. It is also worth noting that the new model is also adapted for the rest results of the typical bridge decks, which also have a well-fitting effect.

7. Conclusions

The spanwise incomplete correlation behaviors of the buffeting forces acting on three typical bluff bridge decks were investigated via a series wind tunnel tests of the synchronous pressure measurement. Some influence factors were considered in the wind tunnel test, such as the turbulence intensity of the turbulent wind flow, the wind attack angle, the wind speed and the separated distance between two sections. The test results were analyzed in detail and some major conclusions were drawn as follows:

(1) The spanwise root coherence of the drag force agrees with that of incidence turbulence in some range of the reduced frequency but there is disagreement for the mostly reduced frequency. The spanwise root coherences of the lift force and the torsional moment are much larger than that of the incidence turbulence. Thus, it was proved once more that the spanwise correlations of the buffeting forces are much better than the spanwise correlations of the fluctuating wind speeds of the incident wind turbulence.

(2) The influence of the wind speed on the correlations of the buffeting forces is slight and it can be ignored in the wind tunnel test as long as the signal-noise ratio is large enough. The influence of the wind attack angle is also somewhat negligible and the spanwise root coherence can be investigated under a wind attack angle of 0°for convenience.

(3) The spanwise coherence of the single flat box deck

is only lightly affected by the turbulence intensity. However, for a blunt bridge deck such as the central slotted box deck, the higher the turbulence intensity is, the stronger the coherence will be. In connection with this, it is suggested that the wind tunnel test should be conducted in the corresponding wind flow field of the real bridge.

(4) The spanwise coherence function often involves several narrow peaks due to the signature turbulence effect in the high reduced frequency zone. These peaks often appear, especially for the blunt bridge deck such as the central slotted box deck and the leeward box of the two-separated paralleled box deck.

(5) The spanwise coherence function is related to the spanwise separation distance and the spanwise integral length scales, and the signature turbulence effect is related to the deck-width-related reduced frequency. Therefore, a rational fraction model with two variables was suggested, and the model proved to be feasible and effective for fitting the test data including the signature turbulence effect.

Acknowledgements

The authors wish to acknowledge the financial support from the National Nature Science Foundation of China (51308330) and the National Science Foundation of Guangdong province (Grant No. 2018A030307008). The support involving the wind tunnel test from the state key laboratory for disaster reduction in civil engineering at Tongji University is particularly appreciated. Any points and concluding remarks presented in this paper are entirely those of the authors.

References

Argentini T., Rocchi D., Muggiasca S. and Zasso A. (2012), "Cross-sectional distributions versus integrated coefficients of flutter derivatives and aerodynamic admittances identified with surface pressure measurement", *J. Wind Eng. Ind. Aerod.*, **104-106**, 152-160. https://doi.org/10.1016/j.jweia.2012.03.009.

Chen, X.Z. (2015), "Analysis of multimode coupled buffeting response of long-span bridges to nonstationary winds with force parameters from stationary wind", *J. Struct. Eng.*, **141**(4), 04014131-1- 04014131-14. https://doi.org/10.1061/(ASCE)ST.1943-541X.0001078.

Chen, X.Z. and Kareem, A. (2002), "Advances in modeling of aerodynamic forces on bridge decks", *J. Eng. Mech.*, **128**, 1193-205. https://doi.org/10.1061/(ASCE)0733-9399(2002)128:11(1193).

Chen, Z.Q., Han, Y., Hua, X.G. and Luo, Y.Z. (2009), "Investigation on influence factors of buffeting response of bridges and its aeroelastic model verification for Xiaoguan Bridges", *Eng. Struct.*, **31**, 417-431. https://doi.org/10.1016/j.engstruct.2008.08.016.

Choi, S.W. and Kim, H.K. (2008), "Design of aerodynamic stabilizing cables for a cable-stayed bridge during construction", *Wind Struct.*, **11**(5), 391-411. https://doi.org/10.12989/was.2008.11.5.391.

Costa, C. (2007), "Aerodynamic admittance functions and buffeting forces for bridges via indicial functions", *J. Fluids Struct.*, **23**, 413-428. https://doi.org/10.1016/j.jfluidstructs.2006.10.002.

Davenport, A.G. (1962), "Buffeting of a suspension bridge by storm winds", *J. Struct. Eng.*, **8**, 233-269.

Davenport, A.G., King, J.P.C. and Larose, G.L. (1992), "Taut strip model tests", *Proceedings of the International Symposium on Aerodynamics of Large Bridges*. Copenhagen, Denmark, February.

Han, Y., Chen, Z.Q. and Hua, X.G. (2010), "New estimation methodology of six complex aerodynamic admittance functions", *Wind Struct.*, **13**(3), 293-307. http://doi.org/10.12989/was.2010.13.3.293.

Hjorth-Hansen, E., Jakobsen, A. and Strommen, E. (1992), "Wind buffeting of a rectangular box girder bridge", *J. Wind Eng. Ind. Aerodyn.*, **41-44**, 1215-1226. https://doi.org/10.1016/0167-6105(92)90128-W.

Hu, L., Xu, Y.L. and Huang, W.F. (2013), "Typhoon-induced non-stationary buffeting response of long-span bridges in complex terrain", *J. Struct. Eng.*, **57**, 406-415. https://doi.org/10.1016/j.engstruct.2013.09.044.

Irwin, P.A. (1997), "Wind tunnel and analytical investigations of the response of the Lions' Gate Bridge to a turbulence wind", Report LTR-LA, National Research Council of Canada, National Aeronautical Establishment, 210.

Jain, A., Jones, N.P. and Scanlan, R.H. (1996), "Coupled flutter and buffeting analysis of long span bridges", *J. Struct. Eng.*, **122**,716-725. https://doi.org/10.1061/(ASCE)0733-9445(1996)122:7(716).

Jakobsen, J.B. (1996), "Spanwise structure of lift and overturning moment on a motionless bridge girder", *Proceedings of the 3rd International Colloquium on Bluff Body Aerodynamics and Applications*, Blacksburg, Virginia, U.S.A., July-August.

Larose, G.L. (1997), "The dynamic action of gusty winds on long-span bridges", Ph.D. Thesis, Technical University of Denmark, Lyngby, Denmark.

Li, M., Li, M.S., Zhong, Y.Z. and Luo, N. (2019), "Buffeting response evaluation of long-span bridges with emphasis on the three-dimensional effects of gusty winds", *J. Sound Vib.*, **439**, 156-172. https://doi.org/10.1016/j.jsv.2018.09.057.

Li, Y.L., Wang, D.X., Wu, C.P. and Chen, X.Z. (2014), "Aerostatic and buffeting response characteristics of catwalk in a long-span suspension bridge", *Wind Struct.*, **19**(6), 665-686. https://doi.org/10.12989/was.2014.19.6.665.

Ma, C.M., Wang, J.X., Li, Q.S. and Liao, H.L. (2019), "3D aerodynamic admittances of streamlined box bridge decks", *Eng. Struct.*, **179**, 321-331. https://doi.org/10.1016/j.engstruct.2018.11.007.

Miyata, T., Yamada, H. and Katsuchi, H. (2002), "Full-scale measurement of Akashi-Kaikyo Bridge during typhoon", *J. Wind Eng. Ind. Aerodyn.*, **90**, 1517-1527. https://doi.org/10.1016/S0167-6105(02)00267-2.

Sankaran, R. and Jancauskas, E.D. (1993), "Measurements of cross-correlation in separated flows around bluff cylinders", *J. Wind Eng. Ind. Aerod.*, **49**, 279-288. https://doi.org/10.1016/0167-6105(93)90023-H.

Scanlan, R.H. (1978), "Action of flexible bridges under wind. II: Buffeting theory", *J. Sound Vib.*, **60**, 201-211. https://doi.org/10.1016/S0022-460X(78)80029-7.

Tan, Z.X., Xu, Y.L., Zhu, L.D. and Zhu, Q. (2018), "POD-based spanwise correlation analysis of aerodynamic and aeroelastic pressures on twin-box bridge decks", *J. Fluids Struct.*, **82**, 520-527. https://doi.org/10.1016/j.jfluidstructs.2018.07.019.

Tubino, F. and Solari, G. (2007), "Gust buffeting of long span bridges: double modal transformation and effective turbulence", *Eng. Struct.*, **29**(8), 1698-1707. https://doi.org/10.1016/j.engstruct.2006.09.019.

Won, J.H., Yoon, J.H., Park, S.J. and Kim, S.H. (2008), "Effects of partially earth-anchored cable system on dynamic wind response of cable-stayed bridges", *Wind Struct.*, **11**(6), 441-453. http://doi.org/10.12989/was.2008.11.6.441.

Xu, Y.L., Sun, D.K., Ko, J.M. and Lin, J.H. (2000), "Fully coupled buffeting analysis of Tsing Ma suspension bridge", *J. Wind Eng. Ind. Aerod.*, **85**(1), 1193-1205. https://doi.org/10.1016/S0167-6105(99)00133-6.

Xu, Z.H. (2006), "Turbulent wind action on long span bridges with separated twin-girder decks", Ph.D. Dissertation, Tongji University, Shanghai, China.

Zhu, Q. and Xu, Y.L. (2014), "Characteristics of distributed aerodynamic forces on a twin-box bridge deck", *J. Wind Eng. Ind. Aerod.*, **131**, 31-45. https://doi.org/10.1016/j.jweia.2014.05.003.

Zhu, Q. and Xu, Y.L. (2016), "Stress-level buffeting analysis of a long-span cable-stayed bridge with a twin-box deck under distributed wind loads", *Eng. Struct.*, **127**, 413-433. https://doi.org/10.1016/j.engstruct.2016.08.050.

AD